Operando X-ray absorption tomography for the characterization of lithium metal electrode morphology and heterogeneity in a liquid Li/S cell

Guillaume Tonin[†,‡,§], *Gavin B. M. Vaughan*[‡], *Renaud Bouchet*[*,§], *Fannie Alloin*[*,§,ϟ], *Céline Barchasz*[*,†]

[†] Univ. Grenoble Alpes, French Atomic Energy and Alternative Energies Agency (CEA-LITEN), DEHT, L2PC, F-38054 Grenoble

[‡] ESRF – The European Synchrotron Radiation Facility, Grenoble 38000, France

[§]Univ. Grenoble Alpes, Univ. Savoie Mont Blanc, CNRS, Grenoble INP, LEPMI, 38000 Grenoble, France

[ϟ]Réseau sur le Stockage Electrochimique de l'Energie (RS2E), CNRS, FR3459, 80039 Amiens Cedex, France

Abstract

Lithium/sulfur batteries have been under intense study for the last two decades, due to the high specific capacity promised by elemental sulfur as an active material. Sulfur is also cheap, abundant and non-toxic compared to conventional transition metal oxides. The Li/S electrochemical cell is traditionally composed of a sulfur-based electrode, an organic liquid electrolyte and a lithium metal electrode. Lithium metal technologies have received a renewed interest, due to the light weight and low operating voltage of the lithium electrode, which makes it the ultimate choice to be combined with high-energy positive electrode materials. In this paper, operando X-ray absorption and phase contrast tomography were employed to characterize the lithium metal electrode morphology and heterogeneity in a liquid Li/S cell. It was observed that oxidation of the lithium foil occurs in a heterogeneous fashion with pit formation from the beginning of discharge, with the pits growing in diameter, depth and quantity during the discharge. Using Faraday's law, the local current density distribution was calculated to confirm the strongly heterogeneous behavior of the lithium metal electrode. We demonstrate that decreasing the current density leads to lithium stripping/plating occurring more homogenously, with the formation of a smaller number of pits.

Keywords: Lithium metal, X-ray absorption tomography, Li/S cell

1. Introduction

Since 1991, the performances of lithium-ion (Li-ion) batteries, in terms of energy density and cyclability, has steadily improved. This technology is now mature, with energy densities as high as 260 $Wh.kg^{-1}$ achieved[1]. Still, alternative electrochemical storage systems continue to be sought, in order to overcome the Li-ion technical drawbacks of high cost, dependence on strategic raw materials, and limited gravimetric energy density[2]. Among the different solutions currently under investigation, Lithium/Sulfur batteries (Li/S) have been intensely studied for the last two decades, because elemental sulfur as an active material promises high theoretical specific capacity (1675 $mAh\ g^{-1}$), and is also cheap, abundant and non-toxic compared to conventional transition metal oxides[3].

The Li/S electrochemical cell is traditionally composed of a sulfur-based electrode, an organic liquid electrolyte and a lithium metal electrode. Lithium (Li) metal rechargeable batteries were first studied in the 1970's, but the idea of using a Li metal electrode was discarded rapidly after many safety events occurred during battery operation[4]. Indeed, lithium metal electrodes have been known for the problematic formation of heterogeneous electrodeposits, especially when using liquid-based electrolytes, which lead to short-circuits and possible thermal runaway[5]. In addition, lithium metal is well known for its surface reactivity, leading to the formation of a Solid Electrolyte Interphase (SEI) when immersed in a liquid electrolyte. This SEI is responsible for lithium and electrolyte consumption, enhancement of lithium/electrolyte interface heterogeneities and poor Li cells cyclability[6,7].

Nevertheless, lithium metal technology has received renewed interest, due to its light weight and to the low operating voltage of the lithium electrode, making it one of the most promising negative electrode materials for combination with high-energy positive electrode materials[8]. Mastering the behavior of lithium metal electrodes, in terms of safety and cyclability, will be critical for the development of high energy density systems such as Li/S technology.

While most efforts have been dedicated to the sulfur electrode, more recent studies have focused on the characterization of the metallic negative electrode and its behavior in Li/S-type liquid electrolytes[9,10]. In particular, advanced characterization tools have been applied to the lithium metal

electrode[11], such as X-ray absorption tomography [12–15], cryo-SEM[16–19], atomic force microscopy[20] and X-ray imaging (XRI)[21].

Tomography has already been used to probe the morphological changes of the lithium electrode and the possible formation of dendrites. Taiwo et al.[12] observed pit-like holes on the lithium surface while discharging the cell, and the formation of mossy lithium while plating during charge, leading to an increase of the lithium thickness with repeated cycling. Similar to absorption tomography, Shi et al.[16] used FIB-SEM imaging to characterize the 3D structure of a lithium metal foil under different cycling conditions. They demonstrated that the pitting phenomenon occurs while cycling to a certain critical current density, and that grain boundaries could be the location of pitting initiation due to the fast atomic diffusion in this area. Using phase contrast imaging, Eastwood et al.[22] demonstrated that lithium is plated with a mossy metallic microstructure, which has a high surface area and is dependent on the current density applied. Sun et al. applied synchrotron X-ray tomography to compare the behavior of the lithium metal using different commercial separators[13,15], while Yu et al.[21] applied X-ray imaging to investigate the effects of electrolyte composition on Li plating/stripping and to optimize the cycling conditions. More recently, Magnier et al.[23] applied X-ray tomography to quantify and spatially probe the Li stripping/plating processes in Li symmetric cells using a poly(ethylene oxide)-based solid electrolyte at 80°C. Using an image analysis method based on the creation of 2D maps of electrode thicknesses, they were able to precisely determine the local heterogeneities at the lithium interface and their impact on the electrode microstructure, and finally to map the local current density at both electrodes based on the thickness change during cycling.

In previous work, we have applied *operando* X-ray absorption tomography and X-ray diffraction computed tomography to the characterization of sulfur and lithium electrodes[24,25]. We observed that lack of pressure control of the cell components led to severe lithium electrode "breathing" already during the first cycle, with the formation of a thick and porous lithium layer[25]. To better control the electrode breathing and the pressure applied to the cell components, a specific cell was designed to allow characterization in a representative pressure-controlled airtight environment[24]. In this paper, *operando* X-ray absorption and phase contrast tomography were employed to characterize lithium metal electrode morphology and heterogeneity evolution during cycling in a liquid Li/S cell, using this pressure-controlled cell design.

2. Experimental Details

Positive electrodes were made of carbon-based current collectors (non-woven carbon paper, H2315®, Freudenberg), with a sulfur loading between 3.3 to 3.7 ~ mg_{sulfur} cm^{-2}. Carbon black (Super P®, Imerys) and PVdF 5130 binder (Solvay; 12 %wt solution in N-methyl-2-pyrrolidinone, NMP) were used as additives, in the weight ratios of 80/10/10 wt% (S_8, SuperP®, PVdF). After homogenization, the ink was coated using a doctor blade on the carbon current collector and the electrodes were dried at 55°C during 24h.

A dedicated cell design, shown in Figure 1, was used for the *operando* synchrotron measurements[25]. The inner part of the cell has a 6 mm diameter with electrodes of 5 mm diameter, to lower the necessary scan range. The spring and two stainless steel pistons were used to maintain a controlled pressure on the electrode stack and ensure an airtight seal. In this experiment, the pressure was fixed to 1.2 bar (similar as the pressure applied in a coin cell) using a compression machine. The upper piston was punctured in order to evacuate the internal pressure due to gas compression when assembling the cell. After that, the two pistons were sealed onto the glass tube with glue and maintained in the compressive machine during at least 2 hours.

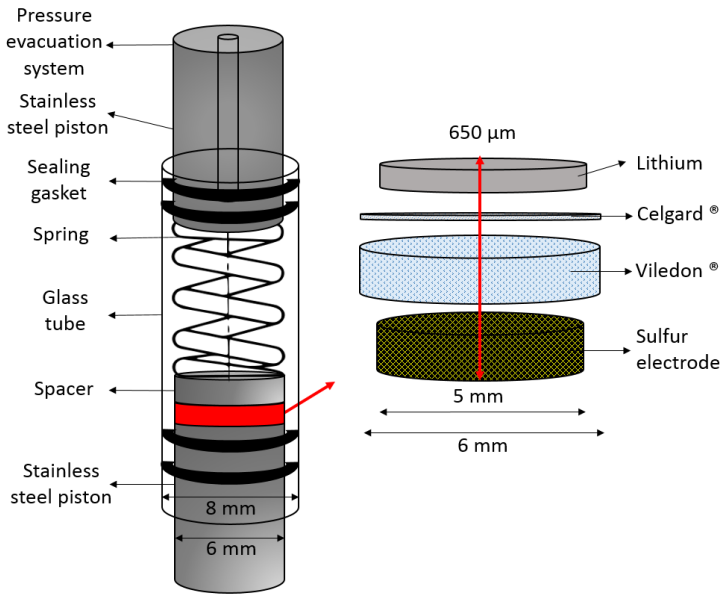

Figure 1. Schematic representation of the pressure-controlled operando cell.

The cell was assembled in a glovebox using a positive electrode, a commercial non treated lithium foil (135 µm thick, Rockwood Li) and a porous separator (Celgard® 2400) combined with an

electrolyte reservoir (Viledon®) soaked with organic electrolyte. The electrolyte was composed of 1 mol L^{-1} of LiTFSI (Aldrich) + 0.1 mol L^{-1} $LiNO_3$ in a mixture of tetraethylene glycol dimethyl ether (TEGDME, dried, Aldrich) and 1.3-dioxolane (DIOX, dried, Aldrich) with 50/50 volume ratio. In these experiments, the electrolyte to sulfur ratio was approximately 20.

Electrochemical tests were carried out with a VMP® biologic battery cycler, in the voltage range of 1.5-3.0 V at three current densities: ~0.23, 0.55 and 1.1 mA cm^{-2}. For clarity, the state of charge and discharge is always given as a function of the practical state of charge (SOC) based on the real capacity of the cell (corresponding to about 50% of the theoretical capacity), whether the system is charging or discharging. *Operando* X-ray absorption and phase contrast tomography measurements were performed at beamline ID15a at the ESRF – The European Synchrotron Radiation Facility[26], with a monochromated incident wavelength of λ=0.1897 Å (energy 65.35 keV). Absorption and phase contrast tomography data were recorded with a periodicity of 30 minutes. The rotation speed was approximately 60 rpm. The measurements were carried out on the whole active part of the cell, a cylinder of 6 mm diameter and 650 µm height. The image resolution for the absorption tomography was 0.717×0.717×0.717 μm^3 per voxel, corresponding to the size of the detector pixel. The software ImageJ with the Fiji plugin was used to segment absorption data. The plugin "Volume viewer" was used to see 3D stack projections of images. XRDCT reconstructions were performed using local codes for filtered back projection point-by-point in the diffraction patterns. After the experiments, the lithium foil was transferred with a special transfer box to a Scanning Electron Microscope (SEM; LEO 1530) in order to observe the morphology.

3. Results and discussion

3.1 Discharge process

The morphological evolution of the lithium metal negative electrode has been characterized over the first discharge under 0.55 mA cm^{-2} (Figure 2). In this figure, vertical tomographic slices shown, illustrating the evolution of the full Li/S cell including the lithium metal electrode morphology at different states of charge (SOC), respectively 50%, 25% & 0% SOC. As observed in Figure 2a, the lithium layer is initially homogenous in density and its surface is flat. The thickness is about 125 µm in average, in good accordance with the supplier specification (135 µm). The separators soaked

with liquid electrolyte are visible from ~200 µm to ~450 µm, while deposited sulfur on the top of the NwC is observed around ~450 µm height.

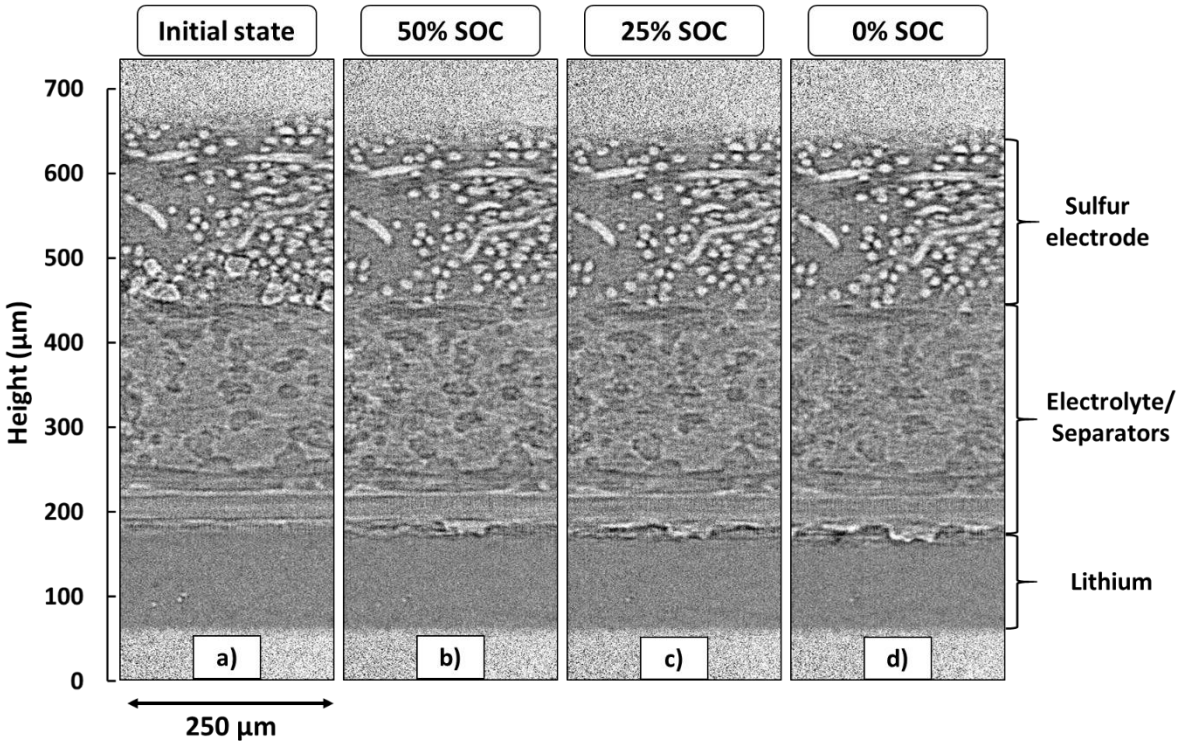

Figure 2: Vertical cross-section of the Li/S operando cell (a) in the initial state (100% SOC), (b) at 1.5 mAh.cm^{-2} (~50% SOC), (c) at 2.17 mAh.cm^{-2} (~25% SOC) (d) at 3.06 mAh.cm^{-2} (0%SOC) i.e. the end of the first discharge. Current density 0.55 mA.cm^{-2}

Already for low state of discharge (~50% SOC or ~1.50 mAh cm^{-2}), it is possible to follow lithium oxidation and see the formation of lithium pits (white regions at the top of the lithium in Figure 2b) due to the non-uniform oxidation of the lithium, a phenomenon already observed in the Li half-cell[24,27] and in other systems[28]. While further discharging the cell (Figures 2c and d), two phenomena are observed: the formation of new pits and the growth, in diameter and slightly in depth, of existing pits, proving that lithium oxidation is more favorable in these areas. Indeed, pitting may lead to SEI cracking due to the interface evolution and fresh lithium being in contact with the electrolyte. Lithium is then more easily oxidized in these highly reactive regions compared to the area where lithium layer is still covered by resistive SEI.

To gain a better picture of the processes, and thanks to the use of high resolution and phase contrast absorption tomography data, it was possible to make a quantitative analysis on the lithium/electrolyte interface. The lithium/electrolyte interface was segmented slice by slice, and

these slices were stacked in order to produce 3D representations of the lithium/electrolyte interface (Figure 3). Following the segmentation, the distance between the bottom of lithium electrode and the lithium/electrolyte interface was calculated for each voxel defined in a 2D (x,y) view. Then, a colormap was used to show the distribution of this distance as shown in Figure 3. The distance between the bottom of lithium electrode and the interface is represented by a purple to white color scale, with white representing the lower depth of oxidation and purple the deeper one.

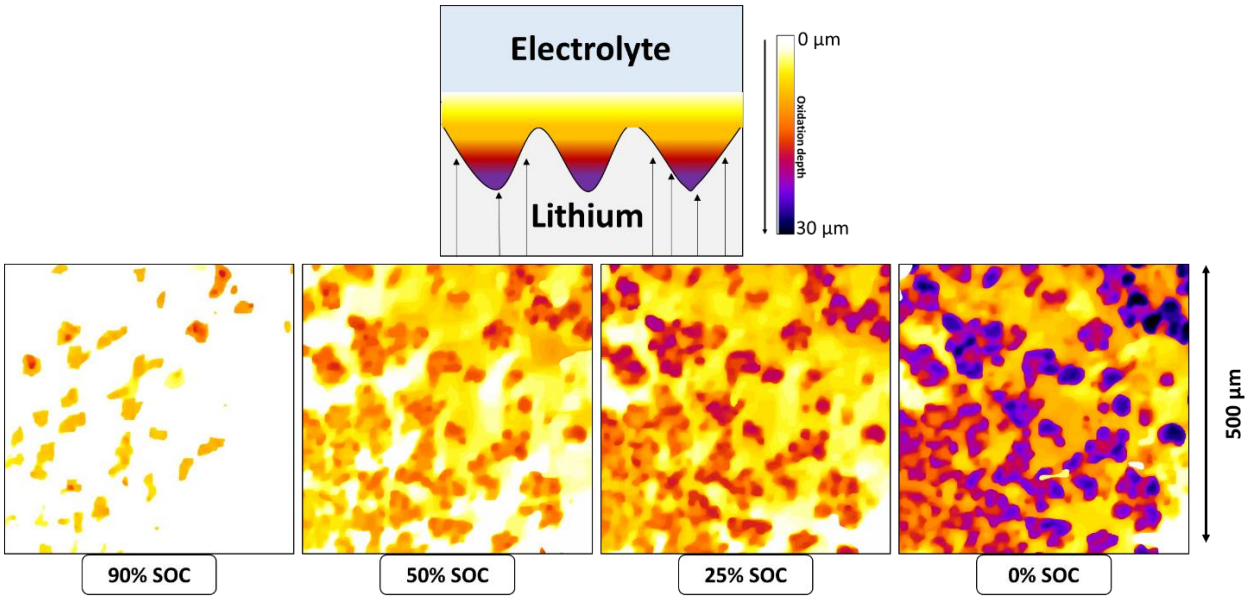

Figure 3. 2D maps (bottom) of the distance between lithium/electrolyte interface and the bottom of lithium electrode, at different states of discharge. A schematic representation (top) of the color scale used in the maps.

The four images taken at 90%, 50%, 25 and 0% SOC are drawn with a common color scale. At 90% SOC, at the beginning of discharge, the lithium interface is smooth and flat, but several pits are already created. At 50% SOC, a large number of pits of moderate depth have already been formed, unpitted areas still remain. From 25% SOC, all existing pits grow in diameter and in depth, and a limited number of new pits have been created compared to 50% SOC.

At the end of the first discharge, the average thickness of the lithium electrode has decreased by about 16 µm. This decrease was calculated by integrating the average distance of the interface for each pixel at the end of the discharge from the initial position of the interface. This value is in good agreement with the 15 µm thick lithium layer expected according to the coulometry (~3.06 mAh cm^{-2}), indicating that the surface analyzed is representative of the expected overall behavior. However, the behavior of the electrode is highly heterogeneous. The pits are on average 30-35 µm

in diameter with a depth of approximately 30 µm with some parts of the electrode (white zones at 90% SOC to light orange at 0% SOC) having limited or no electrochemical activity, even if this represents a minority of the electrode surface.

These results show the strong heterogeneity of the lithium surface reactivity, already from the beginning of the stripping, despite the use of a pressure-controlled cell. This probably reflects the heterogeneity of the solid electrolyte interphase (SEI)[29].

To understand the origin of these heterogeneities, and based on the methodology developed by Magnier et al.[23], a map of the current density distribution was calculated for each SOC, considering that pit depth is proportional to the local current density in the cell, with the average oxidation depth corresponding to the mean current density of 0.55 mA cm^{-2} (the current density applied to the cell). The distributions of local current densities at 90%, 25% and 0% SOC are shown in Figure 4.

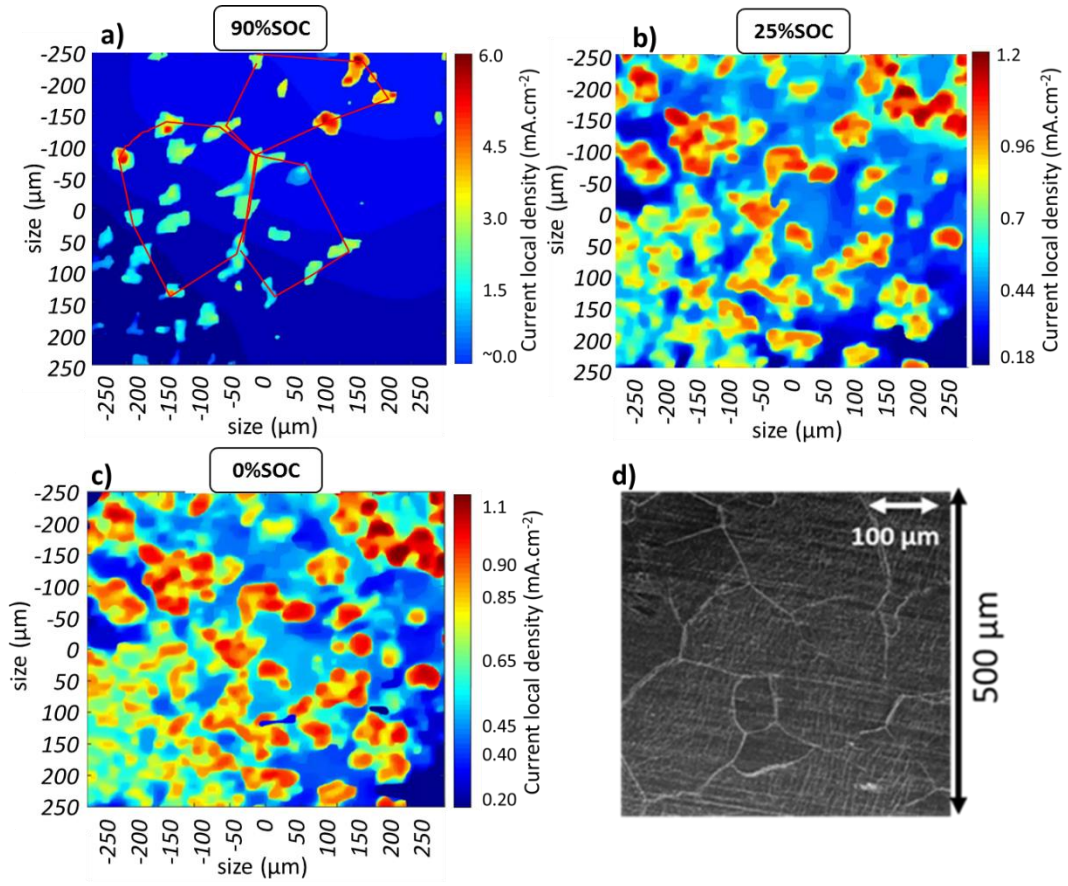

Figure 4. Estimated local current density distributions at a) 90% (the red lines are only a guide for the eyes), b) 25% and c) 0% SOC. Bottom-right) SEM observation of the lithium foil microstructure. The color scales are not the same for all the figure and indicated in each image.

This map shows a very broad current density distribution already at the beginning of discharge (90% SOC), with local current densities as high as ~6 mA cm^{-2} while some areas are completely inactive. This figure shows that lithium pitting is severe at the beginning of discharge, with preferential stripping in some very localized lithium surface areas. Lithium pitting keeps forming during the discharge, with similar geometries of heterogeneities at 50% SOC, resulting in a lower dispersion of the current density (from ~0 mA cm^{-2} to ~1.2 mA cm^{-2}). At 0% SOC, heterogeneities are still clearly visible, resulting in a broad current density distribution, with values varying from 0.2 mA cm^{-2} to 1.1 mA cm^{-2} while the imposed value is equal to 0.55 mA cm^{-2}. Interestingly, by comparing the position of pits on the lithium surface and the location of higher sulfur content[24] in the positive electrode, this distribution cannot be directly linked to the initial sulfur distribution, and therefore does not seem to come from cross-talk between the two electrodes. On the contrary, the SEM image of the lithium foil microstructure (Figure 4d) proves that the initial pitting is likely

to take place preferentially at the grain boundaries[23], as already reported by Shi et al.[16] Indeed, the distribution of the pits at the beginning of the discharge (90% SOC) fits quite well, in term of distribution, with these boundaries. The observation of these large current variations confirms that controlling the lithium initial morphology and its evolution upon cycling remains the major hurdle to be overcome in these systems. In particular, the pressure applied to the cell does not seem to homogenize the response of the lithium metal. Interestingly, most studies in the literature are focused on the reduction process, which is known to lead to heterogeneous lithium electrodeposits. But few concerns the oxidation, which we have seen plays strong role on the lithium plating and can form the seeds of subsequent dendrite growth. This process is analyzed in the next section using the same battery.

3.2 Charge process

Vertical tomographic slices taken during the charging process are presented in Figure 5.

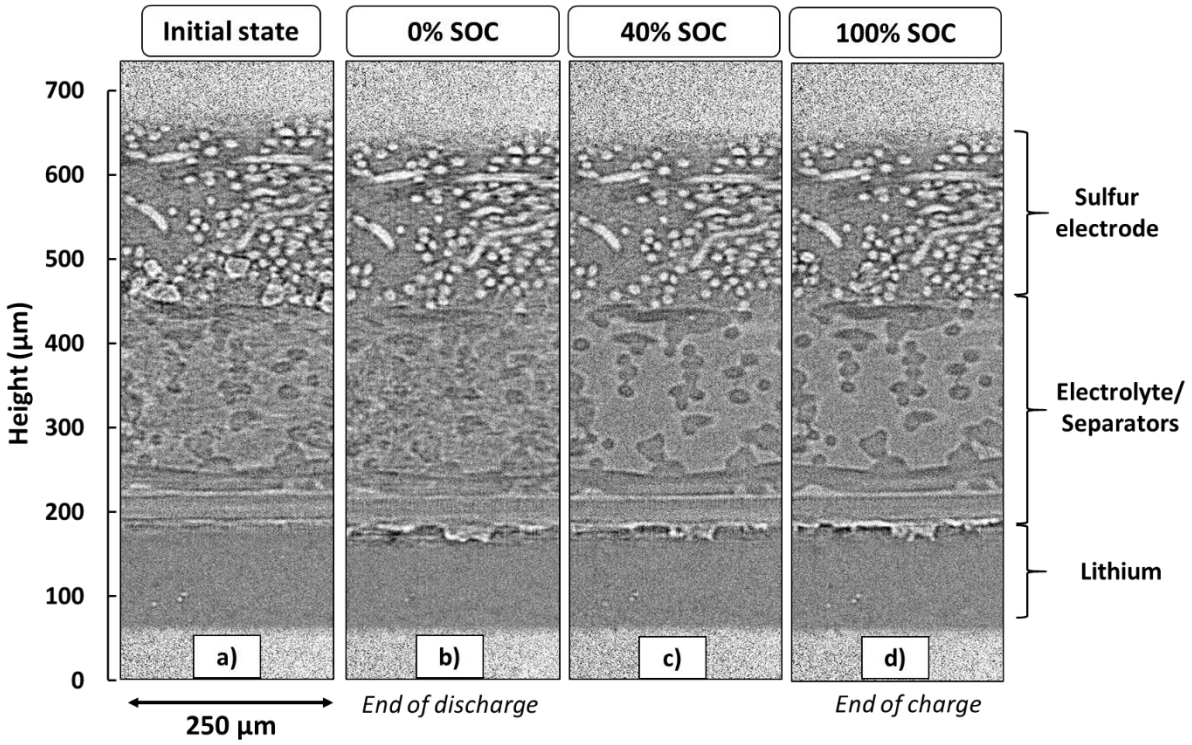

Figure 5: Vertical cross-section of the Li/S operando cell during the first charge: (a) in the initial state before cycling (100% SOC), (b) at the end of the first discharge (0%SOC), (c) at 40% SOC and (d) at the end of the first charge (100% SOC).

As seen in Figure 5, lithium is plated both in the pits formed during the previous discharge as well as onto the lithium surface. In both cases, and despite the use of a slight pressure in the cell (~1.2 bars), lithium is plated in a mossy form with a characteristic high surface area (so-called High Surface Area Lithium), as previously reported[12,22,25]. At the end of charge, the averaged thickness of the lithium deposit is ~17.5 µm compared to the 13 µm expected based on the coulometry, indicating the deposition of a porous lithium morphology. Unfortunately, the investigation of lithium behavior during the charge could not be done in details, as it was barely possible to apply the same segmentation methodology of the interface compared to fresh lithium, and get quantitative analysis from the data.

3.3 Current density investigation

The influence of the current density was investigated with the same methodology, as its impact on lithium plating has already been clearly identified and discussed[30]. The impact of current density on the lithium surface topology in a Li/S cell is of the utmost interest as these electrodes are envisioned to have high surface capacity (3-4 mAh cm^{-2}) thus high current density values even at low C rate. To investigate the influence of current density, an identical cell was cycled at a lower current density of about 0.23 mA cm^{-2} (corresponding to a C-rate equal to C/15), with similar practical capacity corresponding to a similar depth of lithium oxidation (17 µm expected from coulometry).

Quantitative analysis was carried out, similar to the one presented for the higher current density (0.55 mA cm^{-2}). The lithium/electrolyte interface was segmented and the distance between the bottom of lithium electrode and the interface was calculated for each voxel defined in a 2D (x,y) view. Then, a colormap was used to show the distribution of these distances. A 3D representation is shown in order to better visualize the heterogeneous interface (Figure 6). For better visualization, the volume representation of the pits has been reversed, meaning that pits formed in the lithium volume appear as hills in Figure 6. With this low current density (0.23 mA cm^{-2}), the lithium stripping seems to occur in a homogenous way, with a 16 µm homogeneous oxidation at the end of the discharge in good accordance with the number of exchanged electrons (Table 1). In addition, only few objects (pits) have been formed on the lithium surface (Figure 6). Pits created have a diameter of about 10 to 20 µm and a relatively small depth of approximately 10 µm. As for the higher current density, the oxidation is preferential in the pits compared to other lithium surfaces.

Indeed, the few pits created continue growing in diameter and in depth while discharging the cell, but their depth remains limited compared to higher current density.

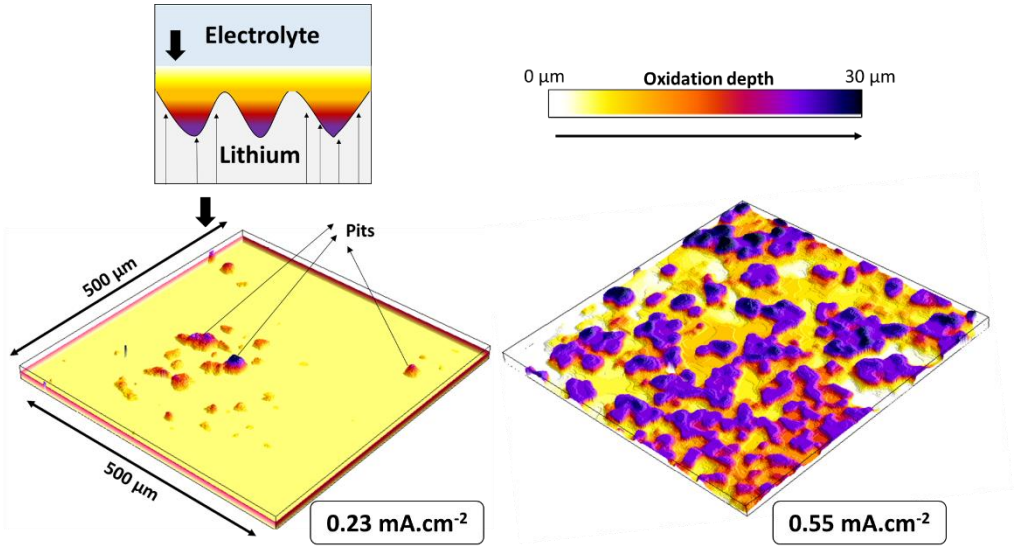

Figure 6. 3D schematic representations of the lithium/electrolyte interface at the end of the first discharge (SOC 0%), at 0.23 and 0.55 mA.cm^{-2} current densities respectively. For better visualization, the volume representation of the pits has been reversed, meaning that pits formed in the lithium volume appear as hills.

Two calculations have been performed to compare to the experimental results (See supplementary information, Figure S3). The first one allowed the measurement of the average reduction of the lithium thickness (labelled "Averaged") taking into account the homogenous and heterogeneous oxidation (in orange, Figure S3). The second one probed solely the thickness corresponding to the complete oxidation of the lithium, *i.e.* not taking into account the pits formed along the interface (labelled "Complete", in green, Figure S3) sums up the experimental parameters and the thickness reduction calculated by both the coulometry and the X-ray tomography measurements. Whereas the complete lithium oxidation, observed at low current density, was coherent with the coulometry, a lower homogeneous oxidation was observed at 0.55 mA cm^{-2}, with only ~5 µm of complete lithium oxidation, *i.e.* only a third of the expected value.

Table 1. Summary of experimental details and analysis of lithium thickness for the different cells (methodology for thickness determination is described in the supplementary information).

Current density (mA cm^{-2})	Capacity (mAh)	Specific capacity (mAh cm^{-2})	Thickness reduction (µm)		
			Coulometry	Experimentally from morphology	
				Averaged	Complete lithium oxidation
0.55	0.6	3.1	15	16	5
0.23	0.69	3.5	17	16	16

During the charge, as observed for higher current density, lithium seems to be plated in the pits already created but also in a homogeneous way, with an increase in lithium thickness of ~15 µm (compared to the 15.7 µm expected with coulometry). This study clearly confirms the strong impact of the current density not only on lithium stripping but also on lithium plating.

3.4 Second cycle

In order to study the effect of the heterogeneities on the lithium surface after a first cycle at high current density (0.55 mA cm^{-2}), the second cycle was also characterized. A 2D representation of the interface at the end of the second discharge is shown in Figure 7 (3D representation is shown in Figure S4). In order to highlight the influence of the heterogeneities, a higher current density was used for the second cycle than for the first one, *i.e.* 1.1 mA cm^{-2} instead of 0.55 mA cm^{-2}.

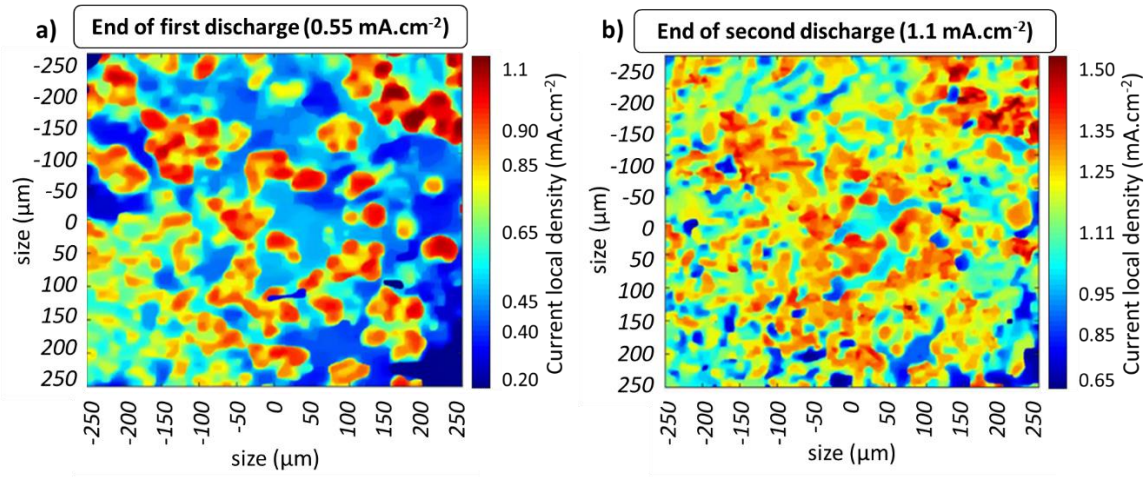

Figure 7. 2D representations of the lithium/electrolyte interface at a) the end of the first discharge (0.55 mA.cm^{-2}) and b) the end of the second discharge (1.1 mA.cm^{-2}).

The interface is more heterogeneous at the end of the second discharge. Pits are formed in the whole surface of the electrode. Interestingly, comparing the 2D images at the end of the first and second discharges, it is clearly visible that pits formed initially at the first discharge remain while new pits spread on the whole lithium surface without any correlation with grains or grain boundaries. The depth of the pits is remarkably the same in both images, *i.e.* 30 µm. Therefore, increasing the current density (1.1 mA cm^{-2} for the second cycle) does not lead to deeper pits, but to an increase quantity of pits. Thus, the lithium heterogeneity starts at the beginning of the cell life and seems to continue during the entire lifetime of the cell.

4. Conclusions

The lithium/electrolyte interface heterogeneity within a Li/S cell has been investigated quantitatively on a complete cycle by means of *operando* X-ray absorption and phase contrast tomography using a pressure-controlled cell design. While the initial lithium layer is dense and homogenous, oxidation of the lithium foil occurs in a heterogeneous way with pit formation at the interface already at the beginning of discharge, with a rapid increase of the lithium surface roughness and the formation of pits of 30 µm in depth. The first pits are created quite rapidly, most likely along the grain boundaries of lithium, and subsequently grow in diameter, depth and number. The behavior of lithium plating seems to be driven by the current density, with much higher heterogeneities and the presence of larger number of pits at high current density. Segmentation of the tomographic data allowed to calculate the variation of lithium thickness at a local scale, and to estimate the local current densities. A very broad current density distribution was observed already at a mean current density of 0.55 mA cm^{-2}, with local values from ~ 0 mA cm^{-2} to ~ 6 mA cm^{-2} at the beginning of discharge. This confirms the strongly heterogeneous behavior of lithium metal, and the need to control the initial lithium morphology and surface quality for viable systems. During the charging process, lithium seems to be plated in the pits already formed and deposits in a mossy form with high surface area. In particular, the pressure range applied to the cell did not seem to improve either the stripping or the plating behavior of lithium metal.

While decreasing the current density, it has been demonstrated that lithium stripping/plating occurs in a more homogenous way, with the formation of a smaller number of pits. In the subsequent discharge, the oxidation is dependent on the previous cycle and the interface becomes more heterogeneous with pitting-like oxidation in the whole surface.

This work demonstrates that understanding the lithium stripping/plating processes is necessary to enhance the cycle life of the lithium metal cells, as a strong evolution of the lithium surface can occur already at the first cycle. The methodology presented here as well as the pressure-controlled cell design are key tools to follow the evolution of lithium heterogeneities while cycling. In the future, the influence of parameters such as higher cell pressure, electrolyte composition, and lithium surface treatments could be investigated using a similar methodology as the one presented here.

Supporting information available

Additional information concerning data treatment can be found in the supporting information.

AUTHOR INFORMATION

Corresponding Author

*E-mail: celine.barchasz@cea.fr Tel: (+33) 4.38.78.90.36

*E-mail: fannie.alloin@lepmi.grenoble-inp.fr Tel: (+33) 4.76.82.66.88

*E-mail: renaud.bouchet@lepmi.grenoble-inp.fr Tel: (+33) 4.76.82.67.77

Author Contributions

C.B, G.T, F.A, R.B contributed to the design of the cell. G.T, G.V set up the experiment, processed and analyzed the data. All authors discussed the results and contributed to the manuscript. F.A, C.B and G.V supervised the whole project.

Notes

The authors declare that they have no competing financial interests.

ACKNOWLEDGMENT

The authors acknowledge CEA-INSTN and the ESRF for Ph.D funding awarded to Guillaume Tonin and thanks ESRF for allocation of beamtime. The authors thank B. Ferrari (LEPMI) for the electrochemical cell realization. This work was performed within the framework of the Centre of Excellence of Multifunctional Architectured Materials "CEMAM" n° AN-10-LABX-44-01.

REFERENCES

1. Armand, M. *et al.* Lithium-ion batteries – Current state of the art and anticipated developments. *Journal of Power Sources* **479**, 228708 (2020).
2. Placke, T., Kloepsch, R., Dühnen, S. & Winter, M. Lithium ion, lithium metal, and alternative rechargeable battery technologies: the odyssey for high energy density. *J Solid State Electrochem* **21**, 1939–1964 (2017).
3. Manthiram, A., Fu, Y., Chung, S.-H., Zu, C. & Su, Y.-S. Rechargeable Lithium–Sulfur Batteries. *Chemical Reviews* **114**, 11751–11787 (2014).
4. Xu, W. *et al.* Lithium metal anodes for rechargeable batteries. *Energy Environ. Sci.* **7**, 513–537 (2014).
5. Cheng, X.-B., Zhang, R., Zhao, C.-Z. & Zhang, Q. Toward Safe Lithium Metal Anode in Rechargeable Batteries: A Review. *Chemical Reviews* **117**, 10403–10473 (2017).
6. Peled, E. The Electrochemical Behavior of Alkali and Alkaline Earth Metals in Nonaqueous Battery Systems. The Solid Electrolyte Interphase Model. *J. Electrochem. Soc.* **126**, 2047 (1979).
7. Liatard, S., Benhamouda, K., Fournier, A., Dijon, J. & Barchasz, C. Influence of catholyte composition on the performances of VACNT/Polysulfides/Li cells. *Electrochimica Acta* **187**, 670–676 (2016).
8. Berg, E. J., Villevieille, C., Streich, D., Trabesinger, S. & Novák, P. Rechargeable Batteries: Grasping for the Limits of Chemistry. *J. Electrochem. Soc.* **162**, A2468 (2015).
9. Zhang, X.-Q., Cheng, X.-B. & Zhang, Q. Advances in Interfaces between Li Metal Anode and Electrolyte. *Advanced Materials Interfaces* **5**, 1701097 (2018).
10. Cao, R., Xu, W., Lv, D., Xiao, J. & Zhang, J.-G. Anodes for Rechargeable Lithium-Sulfur Batteries. *Advanced Energy Materials* **5**, 1402273 (2015).
11. Foroozan, T., Sharifi-Asl, S. & Shahbazian-Yassar, R. Mechanistic understanding of Li dendrites growth by in- situ/operando imaging techniques. *Journal of Power Sources* **461**, 228135 (2020).
12. Taiwo, O. O. *et al.* Investigating the evolving microstructure of lithium metal electrodes in 3D using X-ray computed tomography. *Physical Chemistry Chemical Physics* **19**, 22111–22120 (2017).

13. Sun, F. *et al.* Advancing knowledge of electrochemically generated lithium microstructure and performance decay of lithium ion battery by synchrotron X-ray tomography. *Materials Today* **27**, 21–32 (2019).

14. Adair, K. R. *et al.* Temperature-Dependent Chemical and Physical Microstructure of Li Metal Anodes Revealed through Synchrotron-Based Imaging Techniques. *Advanced Materials* **32**, 2002550 (2020).

15. Dong, K. *et al.* Non-destructive characterization of lithium deposition at the Li/separator and Li/carbon matrix interregion by synchrotron X-ray tomography. *Nano Energy* **62**, 11–19 (2019).

16. Shi, F. *et al.* Lithium metal stripping beneath the solid electrolyte interphase. *Proceedings of the National Academy of Sciences* **115**, 8529–8534 (2018).

17. Qin, L. *et al.* The role of mechanical pressure on dendritic surface toward stable lithium metal anode. *Nano Energy* **77**, 105098 (2020).

18. Zachman, M. J., Tu, Z., Archer, L. A. & Kourkoutis, L. F. Nanoscale Elemental Mapping of Intact Solid–Liquid Interfaces and Reactive Materials in Energy Devices Enabled by Cryo-FIB/SEM. *ACS Energy Lett.* **5**, 1224–1232 (2020).

19. Fang, C. *et al.* Quantifying inactive lithium in lithium metal batteries. *Nature* **572**, 511–515 (2019).

20. Meyerson, M. L. *et al.* The effect of local lithium surface chemistry and topography on solid electrolyte interphase composition and dendrite nucleation. *J. Mater. Chem. A* **7**, 14882–14894 (2019).

21. Yu, S.-H., Huang, X., Brock, J. D. & Abruña, H. D. Regulating Key Variables and Visualizing Lithium Dendrite Growth: An Operando X-ray Study. *J. Am. Chem. Soc.* **141**, 8441–8449 (2019).

22. Eastwood, D. S. *et al.* Three-dimensional characterization of electrodeposited lithium microstructures using synchrotron X-ray phase contrast imaging. *Chemical Communications* **51**, 266–268 (2014).

23. Magnier, L. *et al.* Quantification of the Local Topological Variations of Stripped and Plated Lithium Metal by X-ray Tomography. *ACS Appl. Mater. Interfaces* **12**, 41390–41397 (2020).

24. Tonin, G. *et al.* Multiscale characterization of a lithium/sulfur battery by coupling operando X-ray tomography and spatially-resolved diffraction. *Scientific Reports* **7**, 2755 (2017).

25. Tonin, G. *et al.* Operando investigation of the lithium/sulfur battery system by coupled X-ray absorption tomography and X-ray diffraction computed tomography. *Journal of Power Sources* **468**, 228287 (2020).

26. Vaughan, G. B. M. *et al.*, ID15A at the ESRF – a beamline for high speed operando X-ray diffraction, diffraction tomography and total scattering Journal of Synchrotron Radiation 27, 515 (2020)

27. Taiwo, O. O. *et al.* Investigating the evolving microstructure of lithium metal electrodes in 3D using X-ray computed tomography. *Phys. Chem. Chem. Phys.* **19**, 22111–22120 (2017).

28. Sun, F. *et al.* Morphological Evolution of Electrochemically Plated/Stripped Lithium Microstructures Investigated by Synchrotron X-ray Phase Contrast Tomography. *ACS Nano* **10**, 7990–7997 (2016).

29. Yoon, G., Moon, S., Ceder, G. & Kang, K. Deposition and Stripping Behavior of Lithium Metal in Electrochemical System: Continuum Mechanics Study. *Chem. Mater.* **30**, 6769–6776 (2018).

30. Brissot, C., Rosso, M., Chazalviel, J.-N. & Lascaud, S. Dendritic growth mechanisms in lithium/polymer cells. *Journal of Power Sources* **81–82**, 925–929 (1999).